Experimental Evaluation on Observer-Based Delay-Compensating Active Damping for LC-Filters

Michael Schütt, Hans-Günter Eckel
UNIVERSITY OF ROSTOCK
Albert-Einstein-Str. 2
D-18059 Rostock, Germany
Tel.: +49 (0) 381 – 498 7116
Fax: +49 (0) 381 – 498 7102
E-Mail: michael.schuett@uni-rostock.de
URL: http://www.iee.uni-rostock.de

Acknowledgments

This paper was made within the framework of the research project *Netz-Stabil* and financed by the European Social Fund (ESF/14-BM-A55-0015/16). This paper is part of the qualification program *Promotion of Young Scientists in Excellent Research Associations - Excellence Research Programme of the State of Mecklenburg-Western Pomerania*.

Keywords

«Active Damping», «Current observer», «Discrete-time», «Digital control», «Frequency-Domain Analysis»

Abstract

This work presents experimental results of a discrete-time observer-based delay-compensating active damping technique for LC filters. This method is state-feedback-based and consequently very robust regarding the system parameter such as the grid impedance. Nonetheless, the limits of this strategy are discussed. The experimental setup is a low voltage representation of a 5 MW wind converter. Much know-how was invested in transferring the electrical conditions from high to low power. Particular mention should be made of the adaptation concerning the naturally slower switches in the high voltage and the compensation of the higher damping of the passive components in the low voltage class.

Introduction

[1] presented an active damping technique for LC filters using observers. The paper outlines the premise that state-feedback-based solutions for active damping (such as [1–3]) are inherently more robust regarding the grid impedance compared to forward-path-based strategies (like [4]). Further, [1] explains that merely using state-feedback directly for fast signals such as LC-resonances for active damping can yield inferior results due to delays in the system, such as the computational delay of the controller itself. That paper, consequently, provides an observer-based solution to compensate for the delays in the system. These observer structures can also replace the necessity of a second current sensor stage. The presented outcomes utilize only inverter current and capacitor voltage measurements. Using another current measurement (grid or capacitor current) would decrease the complexity and improve the robustness of the proposed strategy.

This paper presents the experimental results of this observer-based active damping technique and outlines its limits.

Control Technique

Figure 1 illustrates the implemented current control scheme with active damping using a cascaded observer structure as proposed in [1].

Since the grid current is just an estimated disturbance and not an observed state, the observer's estimate-phase lags depending on the observer's controller bandwidth [1]. [1] further argues that the dead-beat observer implementation ensures that the current information lags by one sample step. Therefore, three stages of the cascaded observer structure (for $k+2$ estimations) have to be implemented to establish a proper phase of the estimated grid-current, as shown in Figure 1. Note that a second current sensor stage significantly reduces the observer cascade's effort, and the grid current becomes an observed state instead of an estimated disturbance, yielding much better dynamic properties regarding phase lags and robustness.

However, the third stage of the cascaded observer structure lacks information on the inverter voltage of the sample instance $k+2$. There might be the argument that the future state information and an estimate of the future current reference could also be used to estimate that voltage reference information.

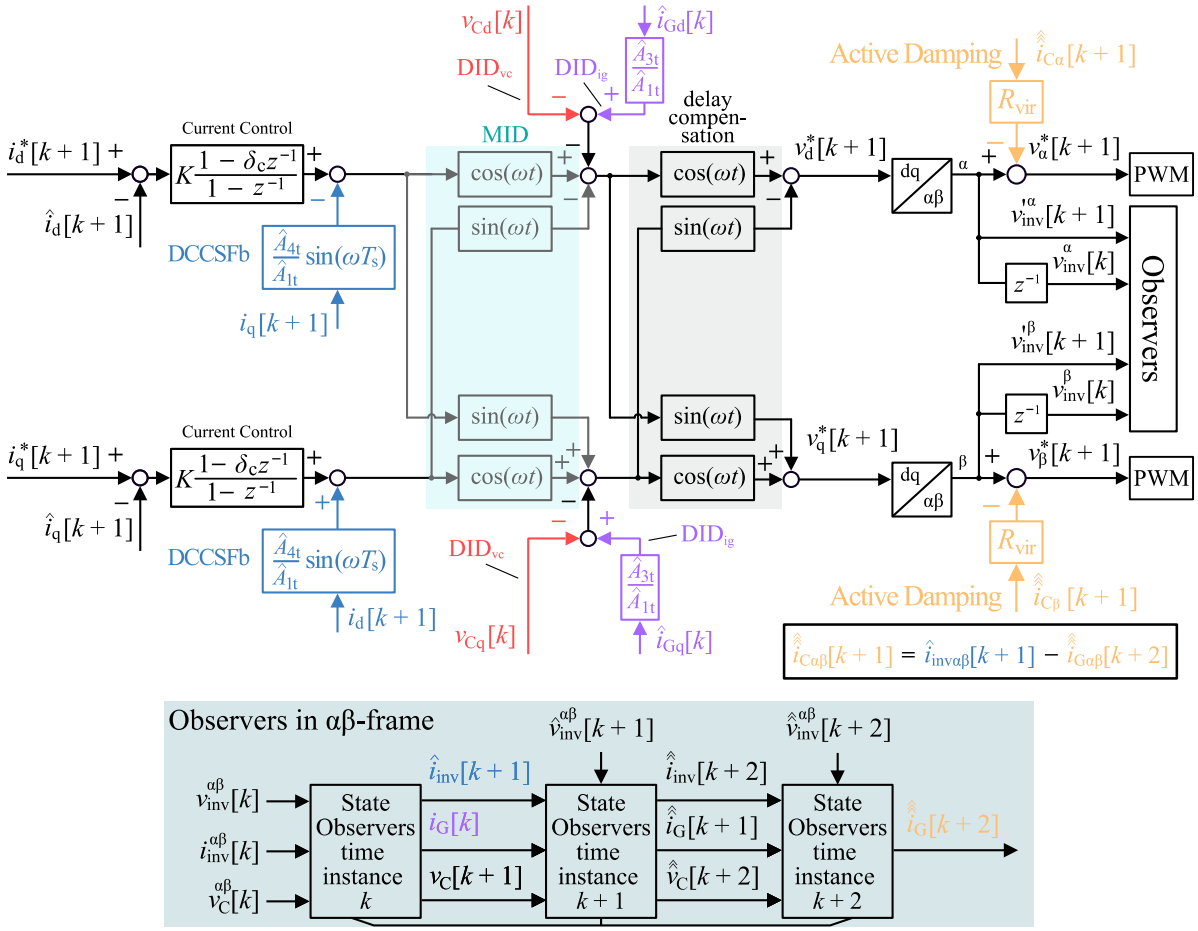

Figure 1: Block diagram of the current control structure with delay compensation via a cascaded Luenberger-style observer structure with active damping implementation and decoupling techniques: DCCSFb – Decoupling Cross-Coupling State Feedback, DIC – Disturbance Input Coupling; DID – Disturbance Input Decoupling (index: vc – capacitor voltage, ig – grid-current). DID – Disturbance Input Decoupling (for: vc-capactor voltage, ig-grid current), MIC – Manipulated Input Coupling (from dq-transformation), MID – Manipulated Input Decoupling (inverse of MIC)

However, using the reference voltage of the previous sample instance does yield very close results already. Investigating the estimation of the voltage reference for the sample instance $k+2$ could be a subject of future research nonetheless.

Simulation Results

The simulation results of this section are based on a 5 MW wind turbine model (parameter in Table 1). This model includes most of the dynamic behavior of the real system down to the switch level – such as computational delay and PWM, yielding an overall dead time of 2 µs.

Figure 2 shows the resulting frequency response estimation plots for varying parameter estimation errors up to 30% with the current control structure of Figure 1 using active damping, disturbance input decoupling, decoupling cross-coupling state feedback based on the present, and future state information estimated from the proposed cascaded discrete Luenberger-style observer structure. It should be noted that no stable operation was found for operation without active damping for 3 kHz sampling (single-sampling) or active damping without delay compensation. The proposed delay compensation structure, however, achieves a very robust and well-damped system.

Experimental Setup

The experimental setup was designed with great care regarding the timing and resistivity of the introduced low voltage components. Very low resistive MOSFETs were chosen to represent the original IGBT switches and slowed down (via gate resistors) to match the switching and conduction behavior.

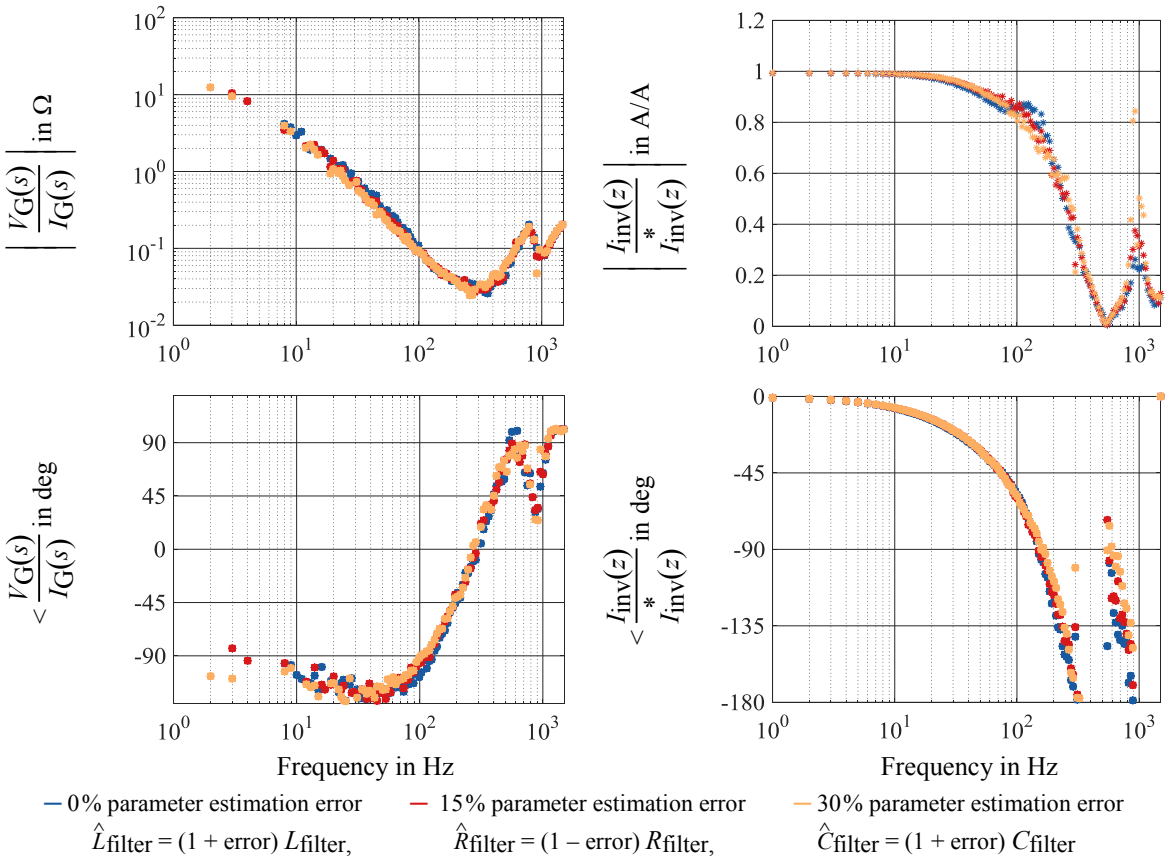

Figure 2: *Simulation*: Dynamic analysis for different parameter estimation errors ($\hat{L}_{filter}$, $\hat{C}_{filter}$, $\hat{R}_{filter}$) of the discrete current controller for LC filters (w/ computational delay and 3 kHz PWM and 3 kHz single-sampling implementation) with active damping (Rvir = 30 mΩ) using a deadbeat-based cascaded discrete Luenberger-style observer structure for estimation of present and future state information for the grid-current, inverter current, and capacitor voltage. *Left*: dynamic stiffness (impedance seen from the grid), *Right*: command tracking (bode-plot)

Table 1 Parameters of the original 5 MW Wind Turbine and the scaled test bench representation

Parameter	5 MW Wind Turbine	25 V Lab test bench
L_f – filter inductance	25 µH	379 µH (400 µH intended)
R_f – filter resistance	0.3 mΩ	18 mΩ (5 mΩ intended)
C_f – filter capacitance	4 mF	240 µF
V_{DC} – DC-link voltage	1100 V	40 V
V_G – grid voltage	690 V	25 V
I_N – base current	4500 A	10 A
C_{DC} – DC-link capacitance	92 mF	5.52 mF
f_{sw} – switching frequency	3 kHz	3 kHz
t_{dead} – dead time (half bridge switching)	appr. 2 µs	appr. 2 µs
Switches	1.7 kV Trench/Fieldstop IGBT 4	100 V HEXFET Power MOSFET

Further, inductive components scale very poorly into low-power applications. This meant that most components off the shelf had too high resistive attributes compared to the original 5 MW reference and thus would dampen the system too much to show any resonant properties. Therefore, the 25V components were overdesigned for their respective currents (factor of 10-100).

With single-sampling, the control was too oscillatory without active damping to find any working operating point. This instability was already present in the simulations.

Figure 3 shows the command tracking plot for different damping coefficients for single-sampling (3 kHz switching and 3 kHz sampling). The grid impedance of the laboratory setup is unknown. Thus, the simulation plots are not exact replicas, but the experiments yield similar attributes and trends. Future work includes both simulation and experimental work to estimate the full-state model of the system more accurately to reproduce the experimental results more closely.

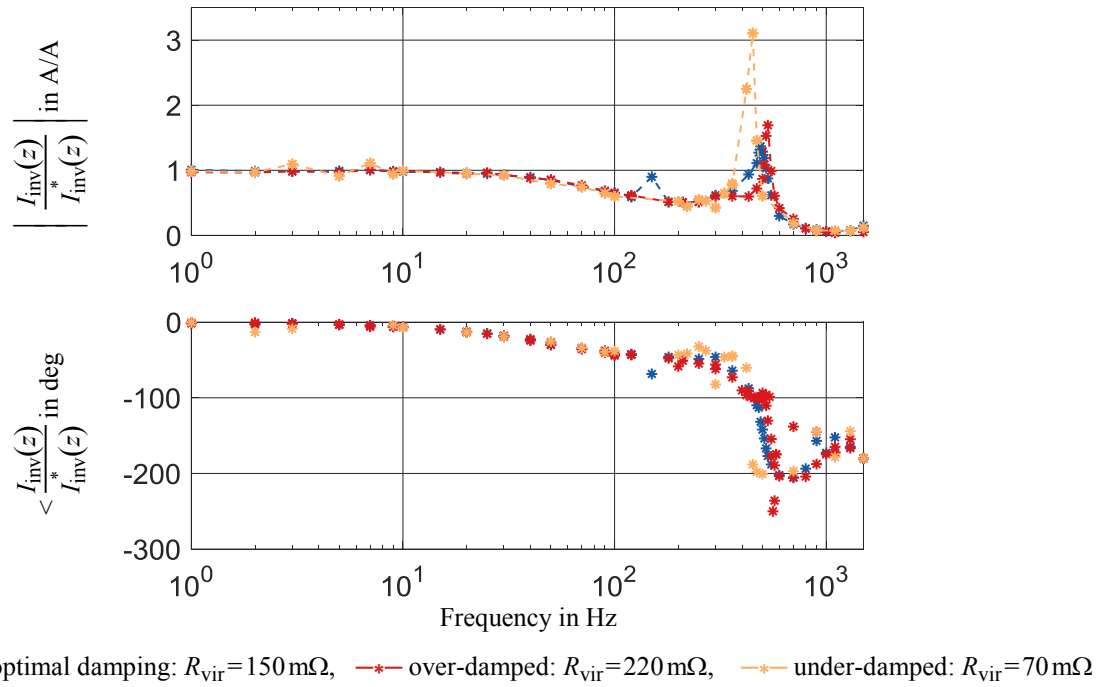

Figure 3: *Measurement*: Command tracking FRF for different active damping coefficients of the discrete current controller for LC filters on the test bench setup (w/ computational delay, 3 kHz sampling) using a deadbeat-based cascaded discrete Luenberger-style observer structure for estimation of present and future state-information for the grid-current, inverter-current, and capacitor-voltage.

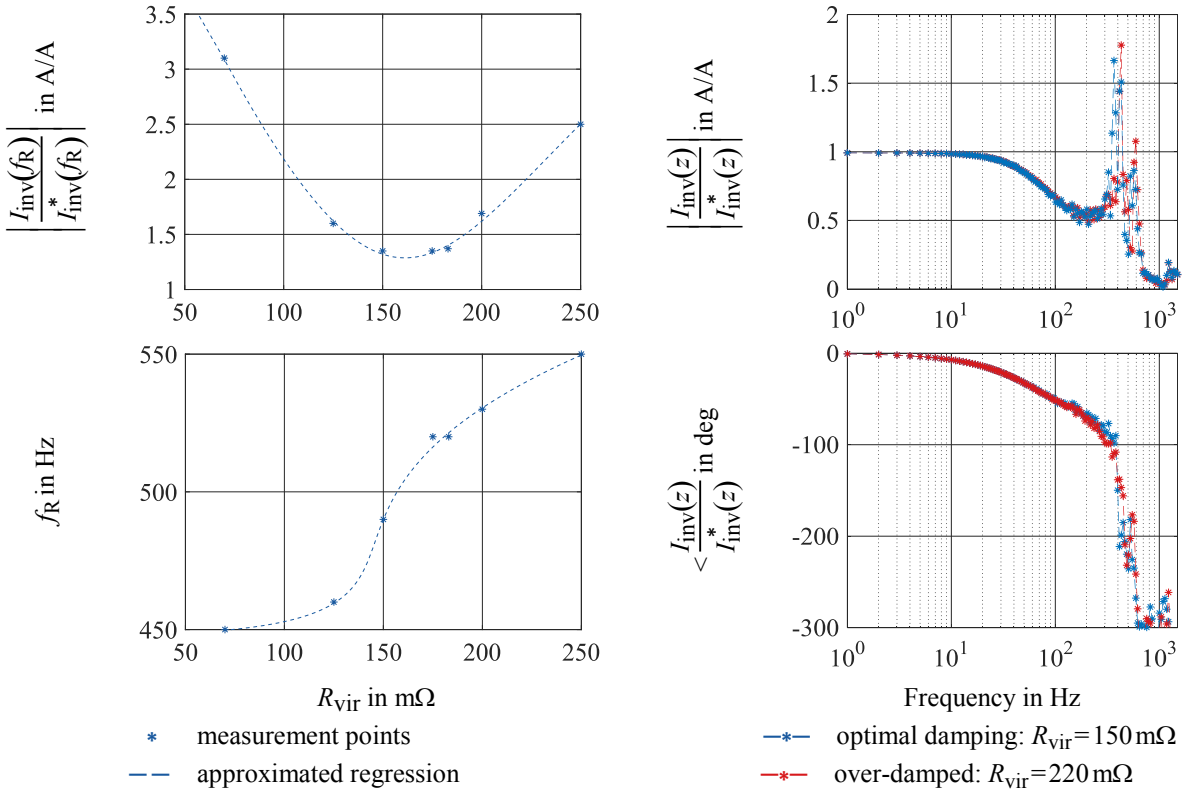

Figure 4: *Left*: *Measurement*: *Top*: Oscillatory peak in the command tracking FRF (*Frequency Response Function*) over the damping coefficient R_{vir}, *Bottom*: Frequency of the oscillatory peak in the command tracking FRF over the damping coefficient – *Right*: *Simulation*: Command tracking FRF with reduced grid-impedance by one order of magnitude – similar behavior to measurements achieved.

In a first attempt, the lab's grid connection is estimated to be an order of magnitude stronger than the original wind turbine application. The anti-resonance is not visible within the Nyquist frequency, which indicates a very low grid-impedance.

This strong grid example seems unrealistic for the given application. However, the effect was investigated further. Figure 4 (right) shows similar attributes in simulations with much smaller grid

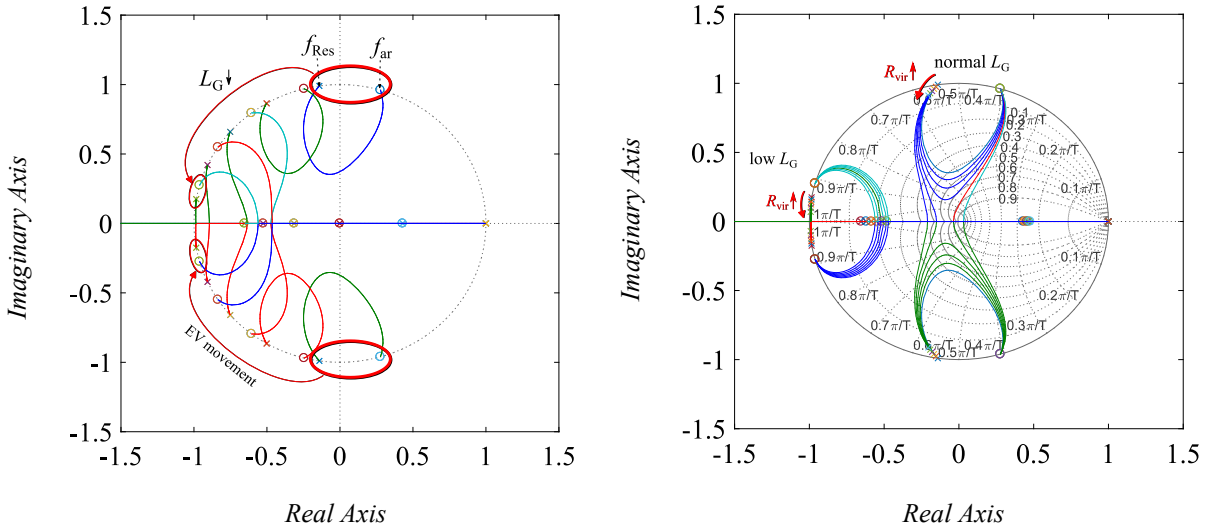

Figure 5: *Left*: eigenvalue movement of the LC-plant for decreasing grid impedance (L_G); *Right*: eigenvalue movement for increasing R_{vir} for two cases of grid impedances (low and normal).

impedances. The location of the EVs depends on the grid impedance. These grid impedances can change over time, but most applications should not drastically change in the order of magnitude.

Figure 5 (left) shows the eigenvalue movement for the variation in grid impedances. Further, Figure 5 (right) shows that lower damping coefficients yield stronger relative eigenvalue movement for a low grid impedance. In this case, over-damping and instability happen much sooner than in the weaker grid example. Figure 4 (left) documents the iterative tuning process of the damping coefficient for the experimental setup.

To summarize, the order of magnitude of the grid impedance dictates the order of magnitude for effective damping coefficients. Therefore, in the case of grid-impedances varying in large regions, adaptive tuning of the damping coefficients is necessary to guarantee stability and well-behaved dynamic attributes for the proposed control scheme.

It should be noted that double sampling (6 kHz sampling for 3 kHz switching) solves most of the discussed issues. The current control was stable even without active damping in that case. However, the produced harmonic impedance of the inverter seen from the grid does not feature the well-damped resonant properties without the active damping (Figure 2 – *left*). A high bandwidth disturbance source must be installed to show these impedance attributes in the test bench case. This hardware implementation is part of the upcoming work.

Figure 6 shows the time domain plots of the α and β inverter currents (grid currents are almost perfect sinusoidal in comparison). The prominent harmonics of the single-sampling version are not caused by the resonance but are in the 150 Hz region (in dq 150 Hz, in αβ in the 100 Hz and 200 Hz region). These issues are caused mainly by the single-sampling PWM scheme, which is discussed in much detail in [5].

Further, measuring currents of inductive components during the maxima and minima of the PWM carrier works very well in filtering out the fundamental switching harmonics. However, using the same sampling instance for the voltage measurement at the capacitors does cause further harmonic issues, which also get attenuated with the double-sampling scheme.

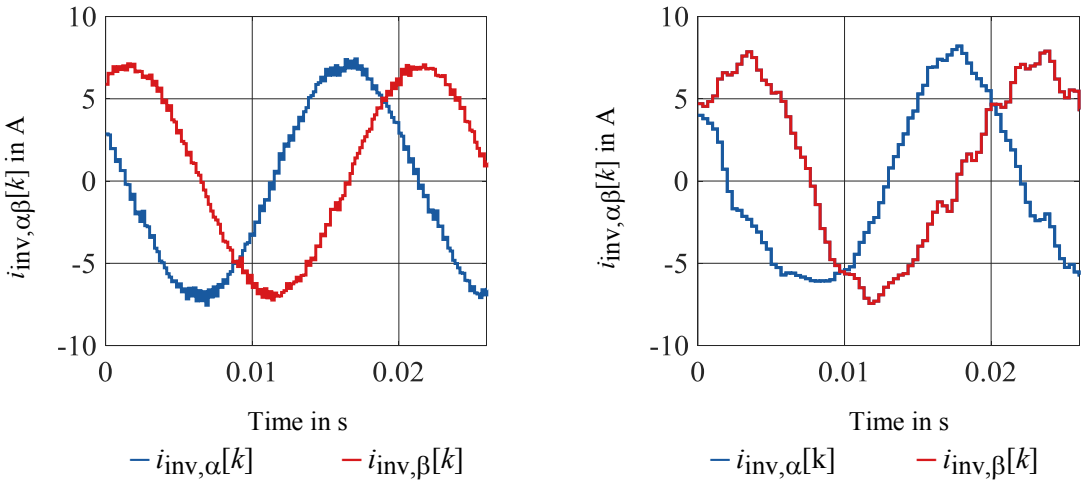

Figure 6: Measurements: Time domain plot of the α,β inverter currents with the proposed current control scheme for 6 kHz double-sampling on the *left* and 3 kHz single-sampling on the *right*.

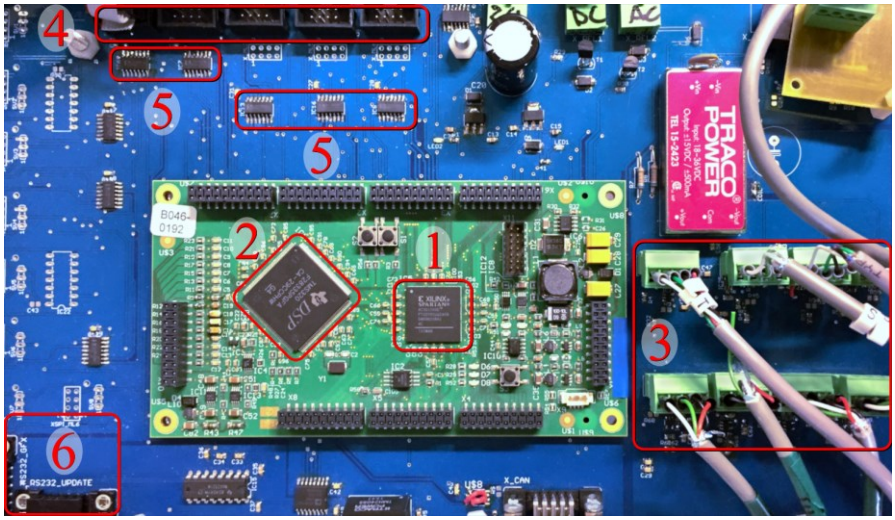

1 – FPGA Xilinx Spartan
2 – DSP TMS320
3 – Sensor inputs (OP-amps)
4 – PWM-output signals
5 – Line driver
6 – RS232: programming & reading

Figure 7: Photographs of the control board of the 25 V test bench − DSP/FPGA combination and peripherals.

Conclusion

This work demonstrates an observer-based algorithm for active damping implemented on a discrete DSP/FPGA-based system (Figure 7 and Figure 8). Furthermore, the design choices are closely linked to the impedance seen from the grid (dynamic stiffness), as this metric provides the most significant insight as to whether actual damping is provided to the overall system. The control structure only measures the inverter current and capacitor voltage. Introducing another current measurement stage would vastly decrease computational effort and dramatically increase overall robustness.

The simulation and experimental results illustrate that the proposed active damping scheme provides vital and dynamically well-behaved damping attributes.

The simulation and experimental results display effective damping of the LC resonance without information on the grid-impedance. While the proposed method does not need the information on the grid impedance, a very strong grid (an order of magnitude smaller than the original setup) still causes issues for the system's stability.

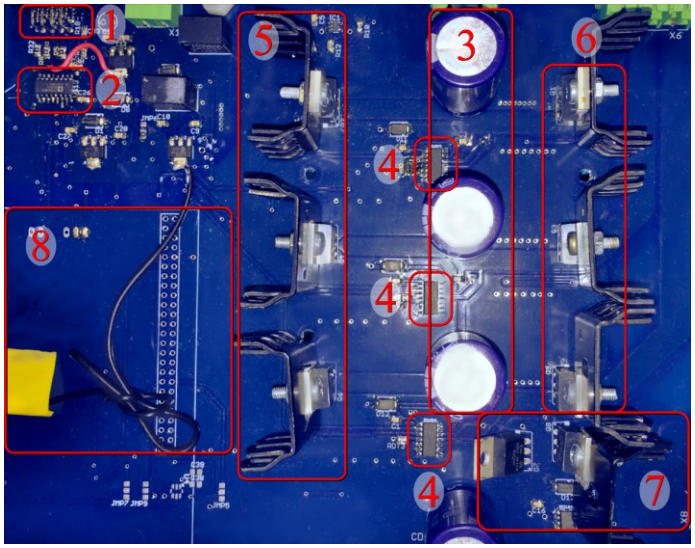

1 – PWM-input signals (from FPGA)
2 – Isolation chips
3 – DC-link
4 – Half-bridge drivers
5 – Low-side phase switches
6 – High-side phase switches
7 – Chopper
8 – Placeholder for alternative microcontroller

Figure 8: Photographs of the inverter board of the 25V laboratory test bench – phase switches, drivers, and peripherals.

References

[1] M. Schütt and H. Eckel, *Discrete active damping control design for LCL-resonances using observers*, 2019 21st European Conference on Power Electronics and Applications (EPE '19 ECCE Europe), 2019, pp. P.1-P.10, doi: 10.23919/EPE.2019.8914981.

[2] B. Abdeldjabar, Xu Dianguo, X. Wang, and F. Blaabjerg, *Robust active damping control of LCL filtered grid connected converter based active disturbance rejection control*, in: 2016 IEEE 8th International Power Electronics and Motion Control Conference (IPEMC-ECCE Asia), 2016, pp. 2661–2666.

[3] H. Ge, Y. Zhen, Y. Wang, and D. Wang, *Research on LCL filter active damping strategy in active power filter system*, in: 2017 9th International Conference on Modelling, Identification and Control (ICMIC), 2017 9th International Conference on Modelling, Identification and Control (ICMIC), 2017, pp. 476–481.

[4] J. Dannehl, C. Wessels, and F.W. Fuchs, *Limitations of Voltage-Oriented PI Current Control of Grid-Connected PWM Rectifiers With LCL Filters*, IEEE Transactions on Industrial Electronics 56 (2009), pp. 380–388

[5] C. M. Wolf, M. W. Degner, and F. Briz, *Analysis of current sampling errors in PWM*, VSI drives, in: 2013 IEEE Energy Conversion Congress and Exposition, 2013, pp. 1770–1777.

[6] B. Abdeldjabar, Xu Dianguo, X. Wang, and F. Blaabjerg, Robust active damping control of LCL filtered grid connected converter based active disturbance rejection control, in: 2016 IEEE 8th International Power Electronics and Motion Control Conference (IPEMC-ECCE Asia), 2016, pp. 2661–2666.

[7] H. Ge, Y. Zhen, Y. Wang, and D. Wang, Research on LCL filter active damping strategy in active power filter system, in: 2017 9th International Conference on Modelling, Identification and Control (ICMIC), 2017 9th International Conference on Modelling, Identification and Control (ICMIC), 2017, pp. 476–481.

[8] H. Yuan and X. Jiang, A simple active damping method for Active Power Filters, in: 2016 IEEE Applied Power Electronics Conference and Exposition (APEC), 2016 IEEE

[9] Hu Wei, Zhou Hui, Sun Jian-jun, Jiang Yi-ming, and Zha Xiao-ming, Resonance analysis and suppression of system with multiple grid-connected inverters, in: 2015 IEEE 2nd International Future Energy Electronics Conference (IFEEC), 2015 IEEE 2nd International Future Energy Electronics Conference (IFEEC), 2015, pp. 1–6.